Proceedings of the Combustion Institute 42 (2026) 106155

Contents lists available at ScienceDirect

Proceedings of the Combustion Institute

journal homepage: www.elsevier.com/locate/proci

From PAH to fullerenes: Closing a nano bowl with a nano lid

Lotefa Binta Tuli [a], Ralf I. Kaiser [b], Alexander M. Mebel [a,*]

[a] Department of Chemistry and Biochemistry, Florida International University, Miami, FL, 33199, USA
[b] Department of Chemistry, University of Hawai'i at Mānoa, Honolulu, HI, 96822, USA

ARTICLE INFO

Keywords:
Polycyclic aromatic hydrocarbons (PAH)
Fullerenes and nanotubes
Reaction mechanism
Equilibrium constant
RRKM theory

ABSTRACT

Quantum chemical DLPNO-CCSD(T)/cc-pVDZ//B3LYP/6–31G(d) calculations have been performed to unravel the formation mechanism of buckminsterfullerene (C_{60}) via the reaction of the C40 nano bowl ($C_{40}H_{10}$) and corannulene ($C_{20}H_{10}$). The generated potential energy surfaces and molecular properties were further utilized to evaluate equilibrium constants and rate constants of elementary chemical reactions involved in the C_{60} synthesis. The overall $C_{40}H_{10} + C_{20}H_{10} \rightarrow C_{60} + 10H_2$ reaction is shown to be highly exoergic and hence thermodynamically favorable at temperatures above 700 K and a kinetically feasible pathway under high-temperature conditions was revealed. This route involves hydrogen atom abstraction steps to activate closed-shell reactants/intermediates alternating with cyclodehydrogenation reactions eventually zipping the edges between the reacting C40 and C20 units by consecutive closures of six- and five-membered rings between them. The reaction is driven/catalyzed by hydrogen atoms which carry out the hydrogen abstractions from $C_{60}H_x$ and are later recovered on the cyclodehydrogenation stages. The initial association reaction, $C_{40}H_9 + C_{20}H_{10} \rightarrow C_{60}H_{18} + H$, linking the two units by a covalent C-C bond appears to represent the kinetic bottleneck of the whole multistep process. This reaction is fast at low temperatures but slows down and has its equilibrium shifted toward the reactants at high temperatures. The feasibility of the proposed mechanism corroborates the hypothesis that C_{60} can be produced through a series of elementary reactions typical for the PAH growth.

Novelty and significance statement: Development of new technologies to produce hydrogen and carbon materials, e.g., thermal or plasma-assisted pyrolysis of natural gas and the gas-phase production of carbon black and nanotubes, requires detailed understanding of the formation of carbonaceous particles from hydrocarbons. While PAHs are firmly established as molecular precursors of carbonaceous particles and their growth mechanisms at the pyrolysis/combustion conditions have been revealed in recent years, the physico-chemical processes leading from small PAHs to fullerenes and nanotubes remain poorly understood. Here, we demonstrate that the formation of C_{60} can be accounted for in terms of PAH growth mechanisms proceeding in a particular order. Our theoretical study reveals a novel thermodynamically favorable and kinetically feasible route for the gas-phase synthesis of C_{60} through a series of elementary chemical reactions typical for the high-temperature PAH growth. While corannulene ($C_{20}H_{10}$) can form from benzene and naphthalene via phenyl addition and cyclization (PAC) and hydrogen abstraction – acetylene addition (HACA) mechanisms and the C40 nano bowl can grow from corannulene by hydrogen abstraction – vinyl acetylene addition (HAVA) reactions followed by cyclodehydrogenations, the nano bowl can be closed by a 'nano lid' $C_{20}H_{10}$ through a series of alternating hydrogen atom abstractions/losses and cyclodehydrogenations zipping the edges between the two units.

1. Introduction

The development of new technologies for the production of hydrogen and carbon materials from fossil and bio fuels, such as thermal [1] or plasma-assisted [2] pyrolysis of natural gas or biomass and the gas-phase production of carbon black [3] and nanotubes [4], requires a detailed understanding of the formation of carbonaceous particles from hydrocarbons in high-temperature environments. As outlined in a recent review [5], polycyclic aromatic hydrocarbons (PAHs) are firmly established as molecular precursors of carbonaceous particles. PAHs form from the initial fuel and their molecular fragments and grow afterwards through chemical reactions taking place at their edges. At high temperatures, PAH moieties start forming clusters and this process eventually ends up in the production of disordered soot particles. In the

* Corresponding author.
E-mail address: mebela@fiu.edu (A.M. Mebel).

https://doi.org/10.1016/j.proci.2026.106155
Received 1 March 2026; Accepted 6 June 2026
Available online 20 July 2026

meantime, minor side products of the soot growth include highly ordered carbon-only containing molecules, such as fullerenes including, e.g., buckminsterfullerene (C_{60}) and rugbyballene (C_{70}). The discovery of fullerenes has paved the path to major scientific research activities in many areas [6,7], including material sciences, medicinal chemistry, physical chemistry, and organic chemistry [8]. While a family of PAH growth mechanisms generally called Hydrogen Activation Carbon Addition (HACA) and including, along with Hydrogen Abstraction aCetylene Addition, Hydrogen Abstraction Vinylacetylene Addition (HAVA), phenyl or phenylacetylene addition and cyclization (PAC/-PhAC), cyclodehydrogenation, and radical-radical recombinations, have been revealed through the synergistic experimental and theoretical studies [5,9–12], the physico-chemical processes leading from small PAHs to ordered carbonaceous nanoparticles (fullerenes, nanotubes) still remain poorly understood. In the present paper, we demonstrate that the formation of C_{60} can be accounted for in terms of the PAH growth mechanisms proceeding in a particular order.

In a recent work [13], we showed that the C40 nano bowl ($C_{40}H_{10}$) can be produced via five consecutive HAVA (benzannulation) steps from corannulene ($C_{20}H_{10}$) forming $C_{40}H_{20}$ followed by five hydrogen atom abstraction – cyclodehydrogenation steps along the edges of $C_{40}H_{20}$ leading to the nano bowl. While the entire mechanism was unraveled theoretically and shown to be feasible, the initial $C_{20}H_9 + C_4H_4$ benzannulation reaction was also probed and verified experimentally in a chemical microreactor. The present paper reveals how the C40 nano bowl can be closed by a C20 'nano lid', $C_{20}H_{10}$, via a similar hydrogen atom abstraction – cyclodehydrogenation zipping mechanism producing buckminsterfullerene C_{60} in the overall $C_{40}H_{10} + C_{20}H_{10} \rightarrow C_{60} + 10H_2$ reaction, which appears to be thermodynamically favorable at high temperatures. Along with calculations of potential energy surfaces (PES) for elementary reaction steps, we characterize their kinetics and equilibria.

2. Computational methods

The molecular parameters including geometries, rotational constants, and vibrational frequencies of various stationary structures (local minima and transition states) on the $C_{60}H_x$ PES (x = 19 – 0) were calculated using the density functional theory (DFT) at the B3LYP/6–31G(d) level [14,15]. Single point energies at optimized geometries were refined employing the domain based local pair-natural orbital singles and doubles coupled cluster method with perturbatively included connected triple excitations (DLPNO-CCSD(T)) [16] with Dunning's cc-pVDZ basis set [17]. The DFT and ab initio calculations were carried out using the GAUSSIAN 16 [18] and ORCA [19] quantum chemistry program packages, respectively. In the earlier work [13], we compared the performance of DLPNO-CCSD(T) with the established chemically accurate G3(MP2,CC) method for the reactions of benzannulation of the corannulenyl radical, $C_{20}H_9 + C_4H_4$, and assessed the convergence of DLPNO-CCSD(T) results with respect to the basis set. A close agreement between the relative energies computed by G3(MP2,CC) and DLPNO-CCSD(T) both with the cc-pVDZ and cc-pVQZ basis sets was found, with the differences normally within 3 kJmol^{-1} with few exceptions. Also, the DLPNO-CCSD(T) results with the cc-pVDZ and cc-pVQZ basis sets were very close. This comparison indicated that the chemical accuracy of about 10 kJmol^{-1} can be normally achieved for molecules of this type employing the DLPNO-CCSD(T)/cc-pVDZ level of theory. Alternatively, the accuracy of DFT relative energies is not sufficient, with discrepancies from the more accurate results often exceeding 40 kJmol^{-1} and not being consistent.

Equilibrium constants for various hydrogen atom abstraction and cyclodehydrogenation reactions were computed within the Rigid-Rotor, Harmonic-Oscillator (RRHO) model. Pressure- and temperature-dependent rate constants for the latter reaction class were evaluated using the Rice–Ramsperger–Kassel–Marcus Master Equation (RRKM-ME) theoretical approach [20] utilizing the MESS software package [21]. Tunneling corrections were included using asymmetric Eckart potentials. The Lennard-Jones parameters ε and σ were estimated based upon the molecular mass of the intermediates involved in each reaction using the formalism proposed by Wang and Frenklach [22] and the parameters for the nitrogen bath gas were taken from Vishnyakov et al. [23]. The collisional energy transfer in ME was treated within the exponential down model [24] where the temperature dependence of the range parameter α for the deactivating wing of the energy transfer function is expressed as $\alpha(T) = \alpha_{300}(T/300\ \mathrm{K})^n$ with $n = 0.85$ and $\alpha_{300} = 247\ \mathrm{cm}^{-1}$ proposed as universal values for hydrocarbons [25]. Supplemental Material (SM) includes MESS input files for the RRKM-ME calculations which incorporate optimized Cartesian coordinates and computed vibrational frequencies for all structures considered in this work.

3. Results and discussion

3.1. Potential energy surfaces and the reaction mechanism

The $C_{40}H_{10} + C_{20}H_{10}$ reaction needs to be initiated by hydrogen atom abstraction from either of the reacting molecules making the $C_{40}H_9$ or $C_{20}H_9$ radicals. Here, we considered $C_{40}H_{10} + H \rightarrow C_{40}H_9 + H_2$ as an option. This reaction is computed to be endothermic by 26 kJmol^{-1} (in terms of ΔH at 0 K) but exoergic (in terms of ΔG) and thus favorable in the forward direction at T = 800 K and above – see Table 1. The rapid kinetics of the direct hydrogen atom abstraction reactions by H atoms from aromatic rings in PAH at combustion temperatures is well established, see e.g. [26], and hence, here we consider only their equilibria described by ΔG values at various temperatures (Table 1).

Once the $C_{40}H_9$ radical is produced, it can react with corannulene. After a barrierless formation of the initial van der Waals complex stabilized by 30 kJmol^{-1} with respect to reactants, the reaction proceeds via a submerged transition state to the covalently bound intermediate $C_{60}H_{19}$ i1 and then is completed by hydrogen atom loss from the attacked carbon atom in $C_{20}H_{10}$ to form $C_{60}H_{18}$ p1 (Fig. 1). Thus, at the end of this stage, the C40 nano bowl gets connected with the C20 nano lid through a single C-C bond. Overall, the $C_{40}H_9 + C_{20}H_{10} \rightarrow C_{60}H_{18} + H$ reaction is computed to be 49 kJmol^{-1} exothermic, with all

Table 1
Reaction enthalpies and Gibbs free energies (kJmol^{-1}) computed at various temperatures.

	ΔH	ΔG			
T, K	0	500	1000	1500	2000
H abstraction, $C_nH_x+H\rightarrow C_nH_{x-1}+H_2$ (a: n = 40; b: n = 60)					
$x = 10^a$	26.0	12.3	−12.5	−42.6	−75.9
$x = 18^b$	44.6	35.0	22.7	11.5	1.5
$x = 16^b$	28.1	19.1	7.0	−4.1	−13.9
$x = 14^b$	23.6	15.1	4.4	−5.3	−13.6
$x = 12^b$	24.6	15.2	2.6	−9.0	−19.5
$x = 10^b$	10.0	2.1	−8.3	−17.5	−25.5
$x = 8^b$	24.0	14.7	2.1	−9.4	−19.8
$x = 6^b$	8.1	−0.4	−11.4	−21.3	−29.9
$x = 4^b$	23.3	13.8	1.3	−10.0	−20.1
$x = 2^b$	−95.1	−106.5	−120.8	−134.2	−146.3
$C_{40}H_9+C_{20}H_{10}\rightarrow C_{60}H_{18}+H$					
	−48.5	−9.4	14.8	34.2	50.6
H loss, $C_{60}H_{x-1}\rightarrow C_{60}H_{x-2}+H$					
$x = 18$	−9.2	−41.3	−78.3	−116.0	−153.8
$x = 16$	105.9	69.5	27.4	−15.6	−58.8
$x = 14$	44.8	9.3	−30.9	−71.8	−112.7
$x = 12$	98.3	59.2	14.4	−31.3	−77.2
$x = 10$	45.6	8.1	−34.1	−77.0	−120.1
$x = 8$	90.4	49.7	3.1	−44.4	−92.0
$x = 6$	65.7	25.5	−19.8	−65.9	−112.2
$x = 4$	−120.5	−157.3	−196.1	−235.1	−274.2
$x = 2$	162.8	135.0	97.9	59.7	21.5
Overall, $C_{40}H_{10}+C_{20}H_{10}\rightarrow C_{60}+10H_2$					
	552.9	169.1	−314.3	−804.7	−1292.1

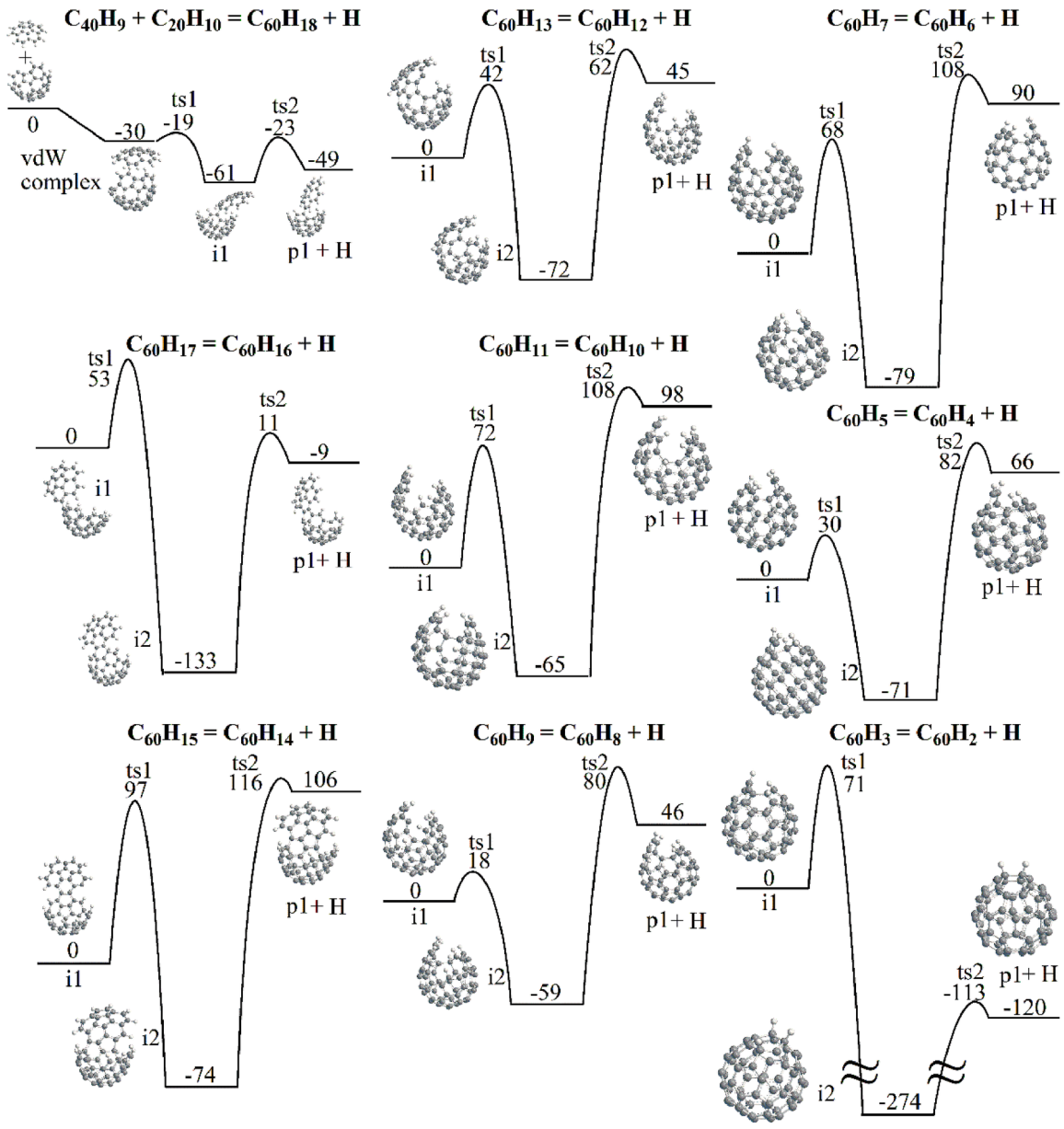

Fig. 1. Potential energy diagrams for cyclodehydrogenation reactions eventually leading from $C_{40}H_9 + C_{20}H_{10}$ to C_{60}. Relative energies for each diagram are shown in kJmol^{-1} with respect to the initial reactant(s) for each stage and are computed at the DLPNO—CCSD(T)/cc-pVDZ//B3LYP/6–31G(d) + ZPE(B3LYP/6–31G(d)) level of theory.

intermediates and transition states residing below the reactants, and thus, is anticipated to be favorable at low temperatures. Note that the same $C_{60}H_{18}$ + H products can be formed through an alternative $C_{40}H_{10}$ + $C_{20}H_9$ reaction. Next, $C_{60}H_{18}$ is activated by hydrogen atom abstraction from the carbon atom in the C20 unit adjacent to the newly formed C-C bond connecting the bowl and the lid endothermic by 44.6 kJmol^{-1}. The first cyclodehydrogenation reaction, $C_{60}H_{17}$ i1 → $C_{60}H_{16}$ p1 + H, ensues (Fig. 1). This reaction proceeds via a six-membered ring closure between the C40 and C20 units through a transition state ts1 illustrated in Fig. 2 and a barrier of 53 kJmol^{-1} The $C_{60}H_{17}$ intermediate i2 resides 133 kJmol^{-1} below i1 and can decompose by the hydrogen atom loss from the former edge of C40 involved in the six-membered ring formation. This results in the $C_{60}H_{16}$ p1 + H products, 9 kJmol^{-1} lower in energy than $C_{60}H_{17}$ i1. Following this stage, the bowl and the lid are linked via a six-membered ring bridge.

Moving further, hydrogen atom abstraction takes place from a carbon atom in the lid close to the six-membered bridge linking the C40 and C20 units, producing $C_{60}H_{15}$ i1. In the latter, a five-membered ring can close between the edges of the units via $C_{60}H_{15}$ ts1 (Fig. 2) leading to i2 and the latter loses an H atom forming $C_{60}H_{14}$ p1 with an indene-like bridge between the bowl and the lid. The $C_{60}H_{15}$ i1 → $C_{60}H_{14}$ p1 + H reaction stage is more energetically demanding as it involves two transition states located 97 and 116 kJmol^{-1} above the reactants and is 106 kJmol^{-1} endothermic overall.

The alternating hydrogen atom abstraction and cyclodehydrogenation steps continue until all hydrogens are removed and the edge between the C40 and C20 units are fully zipped forming the C_{60} ball. Among the cyclodehydrogenation steps, six-membered ring closures take turns with five-membered ring closures (Fig. 1). The steps involving six-membered ring closures ($C_{60}H_{x-1}$ → $C_{60}H_{x-2}$ + H with x = 14, 10, and 6) have relatively low reaction endothermicities of 45–66 kJmol^{-1} and critical barriers for the final hydrogen atom elimination step of 62–82 kJmol^{-1} relative to the decomposing $C_{60}H_{x-1}$ i1 reactant. The steps with five-membered ring closures (x = 12 and 8) require higher

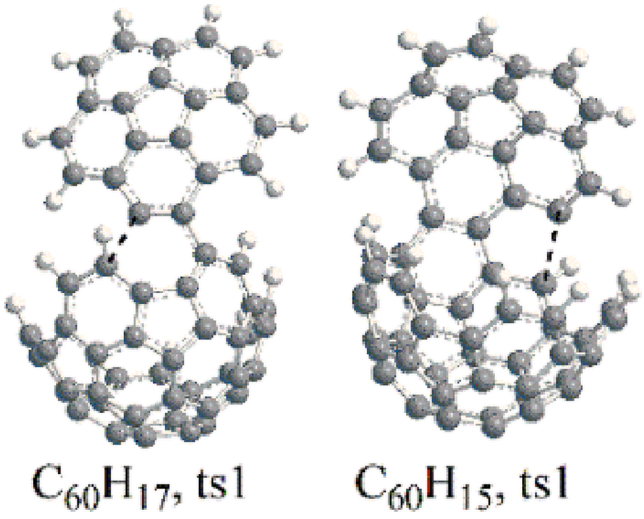

Fig. 2. Structures of transition states for six- and five-membered ring closures.

energy input, with endothermicities of 98 and 90 kJmol^{-1}, respectively, and the hydrogen atom loss barrier of 108 kJmol^{-1} for both. The energetics of the last stages of C_{60} formation are peculiar. The $C_{60}H_3 \rightarrow C_{60}H_2 + H$ reaction is highly exothermic because it involves simultaneous closures of two rings and thus, the formation of a fully closed carbon ball. The hydrogen atom abstraction from $C_{60}H_2$ is also highly favorable (95.1 kJmol^{-1} exothermic, see Table 1) and the final $C_{60}H \rightarrow C_{60} + H$ step is 163 kJmol^{-1} endothermic via a barrier of 172 kJmol^{-1} reflecting a rather week C-H bond.

3.2. Reaction kinetics and equilibria

The overall $C_{40}H_{10} + C_{20}H_{10} \rightarrow C_{60} + 10H_2$ reaction is highly endothermic but becomes exoergic above 700 K and its thermodynamic favorability keeps increasing with temperature due to the high entropic preference for the production of ten H_2 molecules. The series of reactions proposed here, hydrogen atom abstraction from $C_{40}H_{10}$, recombination of $C_{40}H_9$ and $C_{20}H_{10}$, and alternating hydrogen atom abstraction and cyclodehydrogenation steps involving $C_{60}H_x$ (x = 19 – 0) present a kinetically feasible path for the thermodynamically favorable process. The hydrogen atom abstraction reactions by hydrogen atom from aromatics are fast [26]. For example, the recommended generic per site rate constants for hydrogen atom abstraction from a zigzag edge of a PAH at 1500 K are 2.4×10^{-13} and 1.4×10^{-12} cm^3 molecule^{-1} s^{-1} in the forward and reverse directions, respectively. The equilibrium is related to the reaction energies, which, with exception of $C_{60}H_{18}$, are lower than 30–35 kJmol^{-1} typical for planar PAHs [26]. The equilibrium constants for hydrogen atom abstractions at 1500 K are usually in the range of 1.4–5.5, excluding a relatively low value for $C_{60}H_{18}$ (0.4) and a very high one for the strongly exothermic $C_{60}H_2 + H \rightarrow C_{60}H + H$ reaction.

All cyclodehydrogenation reactions are predicted to be fast and thermodynamically favorable at high temperatures (see Fig. 3a and b and Tables 1 and 2). Consider, for example, $C_{60}H_{15} \rightarrow C_{60}H_{14} + H$, which has the highest barriers and endothermicity. At 1 atm, the decomposition rate constant evaluated including contributions from the well-skipping channel and collisional stabilization of i2 followed by its thermal decomposition exceeds 10^6 s^{-1} at $T \geq 1000$ K indicating that $C_{60}H_{15}$ would have a lifetime on a sub microsecond scale (Fig. 3b). At the high-pressure limit and in steady-state conditions, most of the $C_{60}H_{x-1}$ radicals would dissociate faster than in 1 ns (Fig. 3a). Also, the RRKM-ME calculations at 1 atm show that $C_{60}H_{x-1}$ i1 no longer exists as a distinct chemical species and equilibrates with i2 at temperatures above 500 K ($C_{60}H_{13}$, $C_{60}H_9$, $C_{60}H_5$), 700 K ($C_{60}H_{17}$, $C_{60}H_7$, $C_{60}H_3$), 800 K ($C_{60}H_{11}$), and 1400 K ($C_{60}H_{15}$); $C_{60}H$ equilibrates with $C_{60} + H$ above 1500 K. While their i2 isomers formed after the ring closure can typically survive up to T = 1500–2500 K at 1 atm, the hydrogen atom loss rate constants from i2 normally exceed 10^5–10^6 s^{-1} above 1000 K. Considering the fast rate of equilibration in the $C_{60}H_{x-1} \rightarrow C_{60}H_{x-2} + H$ reactions, it is informative to consider equilibrium concentration ratios $[C_{60}H_{x-2}]/[C_{60}H_{x-1}]$ (Table 2). Their values greatly exceed unity even at 500 K for x = 18, 14, 10, and 4 and at 1000 K and above for x = 16, 12, 8, and 6. For the hydrogen atom loss from $C_{60}H$, the equilibrium $[C_{60}H]/[C_{60}]$ ratio becomes larger than 1 at 1300 and 1600 K with hydrogen atom mole fractions of 0.0004 and 0.01 [27], respectively. We have also repeated these calculations for the constant concentration of H atoms, $[H] = 5 \times 10^{15}$ molecule cm^{-3} [28], and the results appeared to be similar to those with $x_H = 0.0004$ (Table S2 in SM); with this value of [H] the $[C_{60}H]/[C_{60}]$ ratio exceeds unity above 1300 K. Summarizing, the $C_{60}H_{x-1} \rightarrow C_{60}H_{x-2} + H$ cyclodehydrogenation reactions are anticipated to be highly favorable in the forward direction under typical combustion and pyrolysis conditions.

It appears that the kinetic bottleneck for the overall $C_{40}H_{10} + C_{20}H_{10} \rightarrow C_{60} + 10H_2$ sequence at high temperatures is the initial $C_{40}H_9 + C_{20}H_{10} \rightarrow C_{60}H_{18} + H$ association step. As seen in Fig. 3c, the computed rate constant at 1 atm in the forward direction (including both the well-skipping mechanism and collisional stabilization/dissociation of the $C_{60}H_{19}$ intermediate) falls with temperature from 1.3×10^{-13} at 500 K to 1.6×10^{-14} and 1.6×10^{-16} cm^3 molecule^{-1} s^{-1} at 1000 and 1500 K, respectively. The stabilization-dissociation mechanism clearly dominates over well-skipping. While this reaction is exoergic below 700 K, its equilibrium constant decreases below unity at higher temperatures,

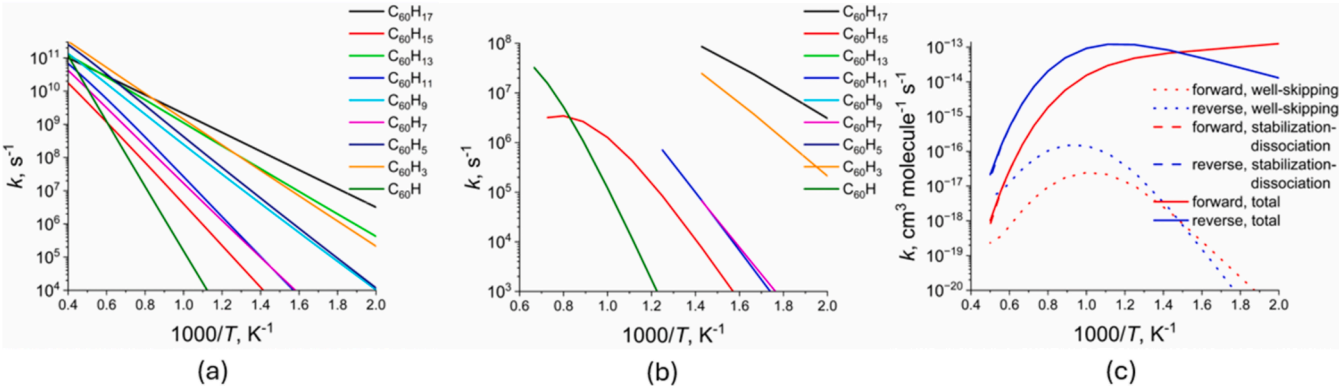

Fig. 3. Calculated rate constants for the $C_{60}H_{x-1}$ (i1) $\rightarrow C_{60}H_{x-2} + H$ reactions: (a) at the high-pressure limit using the steady-state approximation for i2, (b) at 1 atm including both the well-skipping channel and stabilization/dissociation of i2 (within the steady-state approximation); (c) for the $C_{40}H_9 + C_{20}H_{10} \rightarrow C_{60}H_{18} + H$ reaction in forward and reverse directions.

Table 2
Equilibrium concentration ratios $[C_{60}H_{x-2}]/[C_{60}H_{x-1}]$ in the $C_{60}H_{x-1} \rightarrow C_{60}H_{x-2} + H$ reactions at typical flame mole fractions of H atoms x_H [27] and equilibrium constants for the $C_{40}H_9 + C_{20}H_{10} \rightarrow C_{60}H_{18} + H$ reaction at various temperatures.

T, K	500		1000		1500		2000	
x_H	0.0004	0.01	0.0004	0.01	0.0004	0.01	0.0004	0.01
$x = 18$	5.16E+07	2.06E+06	3.09E+07	1.23E+06	2.74E+07	1.10E+06	2.60E+07	1.04E+06
$x = 16$	1.38E-04	5.51E-06	9.25E+01	3.70E+00	8.72E+03	3.49E+02	8.60E+04	3.44E+03
$x = 14$	2.68E+02	1.07E+01	1.03E+05	4.10E+03	7.90E+05	3.16E+04	2.20E+06	8.79E+04
$x = 12$	1.62E-03	6.49E-05	4.43E+02	1.77E+01	3.09E+04	1.23E+03	2.60E+05	1.04E+04
$x = 10$	3.57E+02	1.43E+01	1.51E+05	6.04E+03	1.20E+06	4.81E+04	3.42E+06	1.37E+05
$x = 8$	1.61E-02	6.44E-04	1.73E+03	6.93E+01	8.82E+04	3.53E+03	6.34E+05	2.54E+04
$x = 6$	5.44E+00	2.18E-01	2.72E+04	1.09E+03	4.94E+05	1.98E+04	2.13E+06	8.53E+04
$x = 4$	6.79E+19	2.72E+18	4.39E+13	1.76E+12	3.85E+11	1.54E+10	3.63E+10	1.45E+09
$x = 2$	1.98E-11	7.91E-13	1.92E-02	7.68E-04	2.08E+01	8.32E-01	6.86E+02	2.74E+01
$C_{40}H_9 + C_{20}H_{10} \rightarrow C_{60}H_{18} + H$								
K_{eq}	9.68E+00		1.68E-01		6.44E-02		4.76E-02	

being as low as 0.17 and 0.06 at 1000 and 1500 K, respectively (Table 2).

3.3. Analysis of uncertainties

In addition to the anticipated error bars in the calculated reaction energies, ±10 kJmol^{-1}, the computed values of Gibbs free energies have uncertainties caused by the use of the harmonic oscillator (HO) approximation for evaluation of vibrational partition functions. Some of the molecules considered here have a large number of low frequencies below 100 cm^{-1}; for example, $C_{60}H_{19}$ i1 has five frequencies in the range of 15–80 cm^{-1}. The use of HO for such modes is inaccurate. Noteworthy, none of these low frequency modes can be characterized as internal rotations and hence described as a hindered rotor; the barrier for the rotation around the single C-C bond connecting the C40 and C20 moieties in $C_{60}H_{19}$ i1 was found to be as high as 88 kJmol^{-1} due to the steric hindrance between edge hydrogen atoms. The number of low frequencies rapidly reduces with the cyclodehydrogenation reactions proceeding and falls to one to two for $x = 12$–8 and to zero for the molecules with six or less hydrogens. To assess and partially remove the possible error in treating the low-frequency modes as HOs, Truhlar and his group proposed to raise all low frequencies under 100 cm^{-1} to 100 cm^{-1} and called this approach 'quasiharmonic' or 'anharmonic' calculation [29]. We utilized this quasiharmonic calculation here. Table S1 in SM compares reaction Gibbs free energies computed using the HO and quasiharmonic approximations. The deviations between the results of two calculations are minimal, within few kJmol^{-1}, for all H abstractions and the overall reaction but is more significant for cyclodehydrogenation reactions, especially when the number of H atoms is still high. Not surprisingly, the largest discrepancies are found for the $C_{40}H_9 + C_{20}H_{10} \rightarrow C_{60}H_{18} + H$ reaction, for which the quasiharmonic ΔG value is 20 kJmol^{-1} higher than the harmonic value even at 500 K, and the difference increases to 85 kJmol^{-1} at 2000 K. For $C_{60}H_{17} \rightarrow C_{60}H_{16} + H$, the quasihamonic ΔG values are lower than the harmonic ones from 9 kJmol^{-1} at 500 K to 39 kJmol^{-1} at 2000 K. The deviations decrease for $C_{60}H_{15} \rightarrow C_{60}H_{14} + H$, with the maximal value of 13 kJmol^{-1} at 2000 K, and become insignificant for the further cyclodehydrogenation reactions.

Turning to the reaction rate constants, the use of the quasiharmonic calculation increases the rate constant for the $C_{60}H_{17} \rightarrow C_{60}H_{16} + H$ reaction by factors of 3.7–4.2 in the 500–2000 K temperature range, whereas the increase is much lower for the other cyclodehydrogenations, by factors of 2.1–1.7, 2.6–2.3, 1.5, 1.9–2.0, and 1.15–1.16 for $C_{60}H_{15}$, $C_{60}H_{13}$, $C_{60}H_{11}$, $C_{60}H_9$, and $C_{60}H_7$, respectively, with no changes afterwards. The largest discrepancy is observed for $C_{40}H_9 + C_{20}H_{10} \rightarrow C_{60}H_{18} + H$ (Fig. S1), where the overall rate constants in the forward and reverse directions fall by factors 250–290 and 2.0–1.7, respectively. Summarizing, the uncertainties due to anharmonicity do not affect the main qualitative results of this work. The use of the quasiharmonic approach reduces the thermodynamic and kinetic favorability of the $C_{40}H_9 + C_{20}H_{10} \rightarrow C_{60}H_{18} + H$ reaction but makes the cyclodehydrogenations more favorable.

4. Astrophysical implications

Buckminsterfullerene (C_{60}) was first conclusively detected in planetary nebulae – descendants of carbon rich Asymptotic Giant Branch (AGB) Stars - in 2010 using the infrared capabilities of the Spitzer Space Telescope. The first confirmed identification occurred in the planetary nebula Tc 1 [30]. The presence of C_{60} was established through its characteristic infrared vibrational emission bands at approximately 7.0, 8.5, 17.4, and 18.9 μm, which correspond to its fundamental molecular modes. Since these initial discoveries, additional planetary nebulae like M 1–20, M 1–12, and K 3–54 have been shown to host fullerenes [31].

The environments in which C_{60} is observed are characterized by strong ultraviolet radiation fields generated by hot central stars. These stars typically have effective temperatures between some 30,000 K and >100,000 K. These stars emit photons spanning from about 1 eV in the optical/near-infrared up to and beyond 13.6 eV in the ultraviolet, with some emission extending into the extreme UV. For central stars near 30,000 K, the maximum of the photon energy distribution lies in the far-ultraviolet at energies of approximately 6–8 eV, while for hotter stars approaching 100,000 K the peak shifts toward higher energies, potentially above 20 eV [32]. In practice, much of the highest-energy radiation is absorbed by the surrounding nebular gas, but a strong far-UV field remains, providing the energetic photons necessary for photochemical processing of carbonaceous material. Therefore, in these environments, energetic photons can photodissociate hydrogenated $C_{60}H_x$ intermediates breaking the weakest C-H bonds and producing $C_{60}H_{x-1}$ radicals and leading to rapid formation of C_{60}.

In contrast, C_{60} is generally not observed in ordinary carbon stars, even though these asymptotic giant branch (AGB) stars are the evolutionary progenitors of planetary nebulae. Carbon stars have much cooler photospheres, typically around 2500–3500 K, and their radiation fields peak in the near-infrared at photon energies near 1 eV [33]. They emit negligible ultraviolet radiation compared to planetary nebula central stars. This difference in radiation environment appears to be crucial, and hence strong photon fields in planetary nebulae can in principle drive formation of fullerenes via successive dehydrogenation along with the aforementioned zipper-type mechanism.

Thus, while the raw carbon-rich precursors to fullerenes are synthesized and ejected during the carbon-star (AGB) phase, the transformation into detectable fullerenes appears to occur primarily in the planetary nebula stage. The observation of C_{60} in planetary nebulae, but not commonly in their carbon-star progenitors therefore reflects the critical role of strong ultraviolet radiation fields in driving the chemistry that leads to fullerene formation, potentially via the radical induced 'zipper line' pathway described in the present work.

5. Conclusions

The present study reveals a thermodynamically favorable and kinetically feasible pathway for the gas-phase synthesis of buckminsterfullerene C_{60} via the association of $C_{40}H_{10}$ (the C40 nano bowl) with corannulene $C_{20}H_{10}$ (a nano lid) in high-temperature environments. The initial reaction steps essentially represent a PAC mechanism where the phenyl moiety is surrounded by a carbon skeleton in the $C_{40}H_9$ (or $C_{20}H_9$) radical. Then, the reaction proceeds via a series of alternating hydrogen atom abstraction by hydrogen atoms and cyclodehydrogenation steps. The hydrogen atom abstraction steps activate closed-shell reactants and intermediates to form reactive radicals, whereas the cyclodehydrogenation reactions eventually zip the edges of the reacting C40 and C20 units by consecutively closing six- and five-membered rings between them. The rate-determining step in the overall $C_{40}H_{10} + C_{20}H_{10} \rightarrow C_{60} + 10H_2$ process, which is thermodynamically driven by the entropic preference to produce ten hydrogen molecules, is the initial $C_{40}H_9 + C_{20}H_{10} \rightarrow C_{60}H_{18} + H$ association. This reaction step is only preferable at low temperatures, whereas the equilibrium at high temperatures is shifted toward the reactants. Considering that corannulene can be formed from benzene and naphthalene through a series of PAC and HACA steps and the C40 nano bowl is produced from $C_{20}H_{10}$ through HAVA and cyclodehydrogenations, we have now fully unraveled a potential C_{60} formation mechanism consisting of elementary reactions typical for the PAH growth.

The reaction sequence of the bowl closing with the lid explored here represents only one of multiple possible mechanisms, as hydrogen atom abstractions from the edge of the C20 unit occur in a particular order, each time next to the newly closed ring. In fact, the hydrogen atom abstraction step can happen randomly from different edge carbon atoms of either C40 or C20 units. In the future, it would be interesting to study whether such random hydrogen atom abstractions can lead to full closure ultimately resulting in C_{60}. One interesting case could be when hydrogen atom abstraction in $C_{60}H_{18}$ occurs on the opposite side of the nano bowl (or lid) followed by the formation of the second C-C bond between C40 and C20 without any ring closures. In this case, the nano lid may stay ajar for a prolonged period allowing atoms or small molecules, from noble gases to H_2, HF, N_2, CO, H_2O, and even larger CH_4 and CH_3OH (see, e.g. [34]) to enter the nano bowl and eventually to get trapped inside, while the closing process completes, thus providing a path toward endohedral fullerenes.

The question on how the C40 nano bowl can be efficiently synthesized remains open, although our previous work [13] has shown a plausible route via a series of cyclodehydrogenation reactions commencing with pentabenzocorannulene $C_{40}H_{20}$ [35] formed via the HAVA mechanism from corannulene, operational at high temperatures, e.g., under the flash vacuum pyrolysis (FVP) conditions. For instance, FVP was successfully utilized to synthesize the [5,5] carbon nanotube $C_{50}H_{10}$, a larger analog of $C_{40}H_{10}$, from its precursor – corannulene substituted with five dichlorobenzenes [36]. Although the present calculations identify a thermodynamically favorable and kinetically feasible pathway toward C_{60}, this work alone cannot fully unravel the conditions at which the synthesis of C_{60} would be the dominantly preferable outcome of chemical processes. Instead, our goal here was to discover mechanistic details of one of the possible formation mechanisms of C_{60} and to determine physically justified thermodynamic parameters and rate constants for chemical reactions involved in this mechanism. Although zipper-like mechanisms toward fullerenes were speculated in the past [37,38], the present work is the very first to provide their mechanistic, thermodynamic, and kinetic parameters. Thus, the work contributes to the development of robust and reliable kinetic models for the formation of fullerenes and soot with predictive power. Such kinetic models can eventually answer the question at what conditions the formation of fullerenes is preferable, which particular mechanisms provide significant inputs in their formation, and how the reaction conditions need to be adjusted to achieve maximal yields of the desired products.

CRediT authorship contribution statement

Lotefa Binta Tuli: Investigation, Data curation, Formal analysis. **Ralf I. Kaiser:** Conceptualization, Funding acquisition. **Alexander M. Mebel:** Conceptualization, Data curation, Formal analysis, Supervision.

Declaration of competing interest

The authors declare that they have no known competing financial interests or personal relationships that could have appeared to influence the work reported in this paper.

Acknowledgements

L.B.T. and A.M.M. acknowledge the Instructional & Research Computing Center (IRCC, web: http://ircc.fiu.edu) at FIU for providing HPC computing resources. R.I.K. acknowledges support from the U.S. Department of Energy, Basic Energy Sciences grant DE-FG02-03ER15411.

Supplementary materials

Supplementary material associated with this article can be found, in the online version, at doi:10.1016/j.proci.2026.106155.

References

[1] N. Sánchez-Bastardo, R. Schlögl, H. Ruland, Methane pyrolysis for CO_2-free H_2 production: a green process to overcome renewable energies unsteadiness, Chem. Ing. Tech. 92 (2020) 1596–1609.
[2] J. Diab, L. Fulcheri, V. Hessel, V. Rohani, M. Frenklach, Why turquoise hydrogen will be a game changer for the energy transition, Int. J. Hydrogen Energy 47 (2022) 25831–25848.
[3] L.J.J. Catalan, B. Roberts, E. Rezaei, A low carbon methanol process using natural gas pyrolysis in a catalyticmolten metal bubble reactor, Chem. Eng. J. 462 (2023) 142230.
[4] A. Nadarajah, J.G. Lawrence, T.W. Hughes, Development and commercialization of vapor grown carbon nanofibers: a review, Key Eng. Mater. 380 (2008) 193–206.
[5] M. Frenklach, A.M. Mebel, On the mechanism of soot nucleation, Phys. Chem. Chem. Phys. 22 (2020) 5314–5331.
[6] A. Hirsch, The Chemistry of the Fullerenes, Georg Thieme Verlag, Stuttgart, 1994.
[7] R. Faust, Fullerene model compounds: bowl-shaped aromatic hydrocarbons and cyclophane-based cage molecules, Angew. Chem. Int. Ed. Engl. 34 (1995) 1429–1432.
[8] H.W. Kroto, J.E. Fischer, D.E. Cox, The Fullerenes, Elsevier Science, 2012.
[9] R.I. Kaiser, D.S.N. Parker, A.M. Mebel, Reaction dynamics in astrochemistry: low-temperature pathways to polycyclic aromatic hydrocarbons in the interstellar medium, Ann. Rev. Phys. Chem. 66 (2015) 43–67.
[10] A.M. Mebel, A. Landera, R.I. Kaiser, Formation mechanisms of naphthalene and indene: from the interstellar medium to combustion flames, J. Phys. Chem. A 121 (2017) 901–926.
[11] R.I. Kaiser, N. Hansen, An aromatic universe—A physical chemistry perspective, J. Phys. Chem. A. 125 (2021) 3826–3840.
[12] S.J. Goettl, M. Ahmed, A.M. Mebel, R.I. Kaiser, Molecular mass growth processes to polycyclic aromatic hydrocarbons through radical–radical reactions exploiting photoionization reflectron time-of-flight mass spectrometry, Acc. Chem. Res. 58 (2025) 2682–2694.
[13] L.B. Tuli, S.J. Goettl, A.M. Turner, A.H. Howlader, P. Hemberger, S.F. Wnuk, T. Guo, A.M. Mebel, R.I. Kaiser, Gas phase synthesis of the C40 nano bowl ($C_{40}H_{10}$), Nature Commun. 14 (2023) 1527.
[14] A.D. Becke, Density-functional thermochemistry. III. The role of exact exchange, J. Chem. Phys. 98 (1993) 5648–5652.
[15] C. Lee, W. Yang, R.G. Parr, Development of the Colle-Salvetti correlation-energy formula into a functional of the electron density, Phys. Rev. B 37 (1988) 785–789.
[16] C. Riplinger, B. Sandhoefer, A. Hansen, F. Neese, Natural triple excitations in local coupled cluster calculations with pair natural orbitals, J. Chem. Phys. 139 (2013) 134101.
[17] T.H. Dunning Jr., Gaussian basis sets for use in correlated molecular calculations. I. The atoms boron through neon and hydrogen, J. Chem. Phys. 90 (1989) 1007–1023.
[18] M.J. Frisch, et al., Gaussian 16, Rev. C.1, Gaussian, Inc, Wallingford, CT, 2019.
[19] F. Neese, The ORCA program system, WIREs Comput. Mol. Sci. 2 (2012) 73–78.
[20] Y. Georgievskii, J.A. Miller, M.P. Burke, S.J. Klippenstein, Reformulation and solution of the master equation for multiple-well chemical reactions, J. Phys. Chem. A 117 (2013) 12146–12154.

[21] Y. Georgievskii, S.J. Klippenstein, Master equation system solver [MESS], see, https://tcg.cse.anl.gov/papr, 2016.
[22] H. Wang, M. Frenklach, Transport properties of polycyclic aromatic hydrocarbons for flame modeling, Combust. Flame 96 (1994) 163–170.
[23] A.V. Neimark, P.I. Ravikovitch, A. Vishnyakov, Adsorption hysteresis in nanopores, Phys. Rev. E 62 (2000) R1493–R1496.
[24] J. Troe, Theory of thermal unimolecular reactions at low pressures. I. Solutions of the master equation, J. Chem. Phys. 66 (1977) 4745–4757.
[25] A.W. Jasper, C.M. Oana, J.A. Miller, Third-body" collision efficiencies for combustion modeling: hydrocarbons in atomic and diatomic baths, Proc. Combust. Inst. 35 (2015) 197–204.
[26] A.S. Semenikhin, A.S. Savchenkova, I.V. Chechet, S.G. Matveev, Z. Liu, M. Frenklach, A.M. Mebel, Rate constants for H abstraction from benzo(a)pyrene and chrysene: a theoretical study, Phys. Chem. Chem. Phys. 19 (2017) 25401–25413.
[27] M. Frenklach, A.S. Semenikhin, A.M. Mebel, On the mechanism of soot nucleation. III. The fate and facility of the E-bridge, J. Phys. Chem. A 125 (2021) 6789–6795.
[28] A. Jain, Y. Wang, W.D. Kulatilaka, Effect of H-atom concentration on soot formation in premixed ethylene/air flames, Proc. Combust. Inst. 37 (2019) 1289–1296.
[29] Y. Zhao, D.G. Truhlar, Computational characterization and modeling of buckyball tweezers: density functional study of concave–convex π π interactions, Phys. Chem. Chem. Phys. 10 (2008) 2813.
[30] J. Cami, J. Bernard-Salas, E. Peeters, S.E. Malek, Detection of C_{60} and C_{70} in a young planetary nebula, Science 329 (2010) 1180–1182.
[31] J.J. Díaz-Luis, D.A. García-Hernández, A. Manchado, F. Cataldo, A search for hydrogenated fullerenes in fullerene-containing planetary nebulae, Astronom. Astrophys. 589 (2016) A5.
[32] O. De Marco, A. Zijlstra, R. Szczerba, Planetary Nebulae, Cambridge University Press, 2025, p. 400.
[33] R.F. Wing, The Carbon Star Phenomenon (International Astronomical Union Symposia Volume 177), Springer, 2000, p. 652.
[34] S. Bloodworth, R.J. Whitby, Synthesis of endohedral fullerenes by molecular surgery, Comm. Chem. 5 (2022) 121.
[35] N.J. Smith, Toward the synthesis of a carbon nanotube end-cap: application of a new benzannulation method to the first synthesis of pentabenzo[a,d,g,j,m] corannulene, Boston College Electron. Thesis or Dissert. (2011).
[36] L.T. Scott, E.A. Jackson, Q. Zhang, B.D. Steinberg, M. Bancu, B. Li, A short, rigid, structurally pure carbon nanotube by stepwise chemical synthesis, J. Am. Chem. Soc. 134 (2012) 107–110.
[37] T. Baum, S. Löffler, P. Löffler, P. Weilmünster, K.-H. Homann, Fullerene ions and their relation to PAH and soot in low-pressure hydrocarbon flames, Ber. Bunsenges. Phys. Chem. 96 (1992) 841–857.
[38] C.J. Pope, J.A. Marr, J.B. Howard, Chemistry of fullerenes C_{60} and C_{70} formation in flames, J. Phys. Chem. 97 (1993) 11001–11013.